The First Detection of $^{13}C^{17}O$ in a Protoplanetary Disk: A Robust Tracer of Disk Gas Mass

Alice S. Booth[1] , Catherine Walsh[1] , John D. Ilee[1] , Shota Notsu[2,3] , Chunhua Qi[4] , Hideko Nomura[5,6] , and Eiji Akiyama[7]

[1] School of Physics and Astronomy, University of Leeds, Leeds LS2 9JT, UK; pyasb@leeds.ac.uk
[2] Department of Astronomy, Graduate School of Science, Kyoto University, Kitashirakawa-Oiwake-cho, Sakyo-ku, Kyoto 606-8502, Japan
[3] Leiden Observatory, Leiden University, P.O. Box 9513, NL-2300 RA, Leiden, The Netherlands
[4] Harvard-Smithsonian Center for Astrophysics, Cambridge, MA 02138, USA
[5] Department of Earth and Planetary Science, Tokyo Institute of Technology, 2-12-1 Ookayama, Meguro-ku, Tokyo 152-8551, Japan
[6] National Astronomical Observatory Japan (NAOJ), Osawa 2-21-1, Mitaka, Tokyo 181-8588, Japan
[7] Institute for the Advancement of Higher Education, Hokkaido University, Kita 17, Nishi 8, Kita-ku, Sapporo, Hokkaido 060-0817, Japan; c.walsh1@leeds.ac.uk

Abstract

Measurements of the gas mass are necessary to determine the planet formation potential of protoplanetary disks. Observations of rare CO isotopologues are typically used to determine disk gas masses; however, if the line emission is optically thick this will result in an underestimated disk mass. With the Atacama Large Millimeter/submillimeter Array we have detected the rarest stable CO isotopologue, $^{13}C^{17}O$, in a protoplanetary disk for the first time. We compare our observations with the existing detections of ^{12}CO, ^{13}CO, $C^{18}O$, and $C^{17}O$ in the HD 163296 disk. Radiative transfer modeling using a previously benchmarked model, and assuming interstellar isotopic abundances, significantly underestimates the integrated intensity of the $^{13}C^{17}O$ $J = 3$–2 line. Reconciliation between the observations and the model requires a global increase in CO gas mass by a factor of 3.5. This is a factor of 2–6 larger than previous gas mass estimates using $C^{18}O$. We find that $C^{18}O$ emission is optically thick within the snow line, while the $^{13}C^{17}O$ emission is optically thin and is thus a robust tracer of the bulk disk CO gas mass.

Unified Astronomy Thesaurus concepts: Protoplanetary disks (1300); Planet formation (1241); Astrochemistry (75); Submillimeter astronomy (1647)

1. Introduction

The mass of a disk sets a limit on the material available for forming a planetary system and can influence the mode of giant planet formation. Most disk gas masses rely on observations of CO that are extrapolated to a total gas mass by assuming a constant CO/H_2 abundance ratio in the disk. However, if the line emission is optically thick this will result in an underestimated disk mass (e.g., Bergin & Williams 2017). Spatially resolved line emission from both $^{13}C^{16}O$ and $^{12}C^{18}O$ are now commonly detected in protoplanetary disks and have been used to determine disk gas masses (e.g., Ansdell et al. 2016; Long et al. 2017). The second-most rare CO isotopologue, $^{13}C^{18}O$, has been detected in the TW Hya disk, and this emission has been proposed to be optically thin and traces the disk midplane, whereas the $C^{18}O$ emission is optically thick within the midplane snow line (Zhang et al. 2017). The underestimation of disk gas mass due to optically thick emission will be more significant in more massive gas-rich disks, i.e., those around Herbig Ae/Be stars versus those around T Tauri stars.

Low CO gas masses, with respect to the dust mass, have been consistently measured in disks, and complementary HD observations imply that this is because of the depletion of gas-phase CO in disks relative to that in the interstellar medium (ISM; Bergin et al. 2013; McClure et al. 2016). CO can be depleted from the gas phase via freezeout onto the icy grains in the cold midplane, and subsequent conversion to CO_2 and more complex organic species, e.g., CH_3OH (e.g., Bosman et al. 2018). Additionally, photodissociation via far-UV radiation destroys CO in the upper disk atmosphere, and isotope-selective photodissociation can enhance the various

isotopologue ratios relative to $^{12}C^{16}O$ in the atmosphere (e.g., Miotello et al. 2014). These chemical effects make the conversion from CO gas mass to total gas mass a non-trivial task.

The protoplanetary disk around HD 163296 has been well characterized with the Atacama Large Millimeter/submillimeter Array (ALMA). Band 6 and 7 observations show rings in both the continuum and the CO gas emission (e.g., Isella et al. 2016; Notsu et al. 2019; see Figure 1(a)). There are four proposed $\approx$0.5–2 M_J planets in this disk inferred from the dust and gas rings, and deviations from Keplerian motion in the CO gas kinematics (Isella et al. 2016; Liu et al. 2018; Pinte et al. 2018; Teague et al. 2018). Recently, $\approx$5 au resolution observations of the continuum emission revealed an additional gap and ring in the inner disk as well as an azimuthal asymmetry in one of the previously detected rings (see Figure 1(a); Isella et al. 2018). Hence, the proposed planet-induced structures in the HD 163296 disk make it an excellent observational laboratory to study planet formation.

We present the first detection of $^{13}C^{17}O$ in a protoplanetary disk providing a strong constraint on the CO gas mass in the HD 163296 disk.

2. Observations

HD 163296 was observed with ALMA in Band 7 during Cycle 3 on 2016 September 16 (2015.1.01259.S, PI: S. Notsu). See Notsu et al. (2019) for details on the calibration and self-calibration of the data. The spectral windows have a resolution of 1953.125 kHz. There are 14 $^{13}C^{17}O$ $J = 3$–2 hyperfine structure lines that lie between 321.851 and 321.852 GHz. All
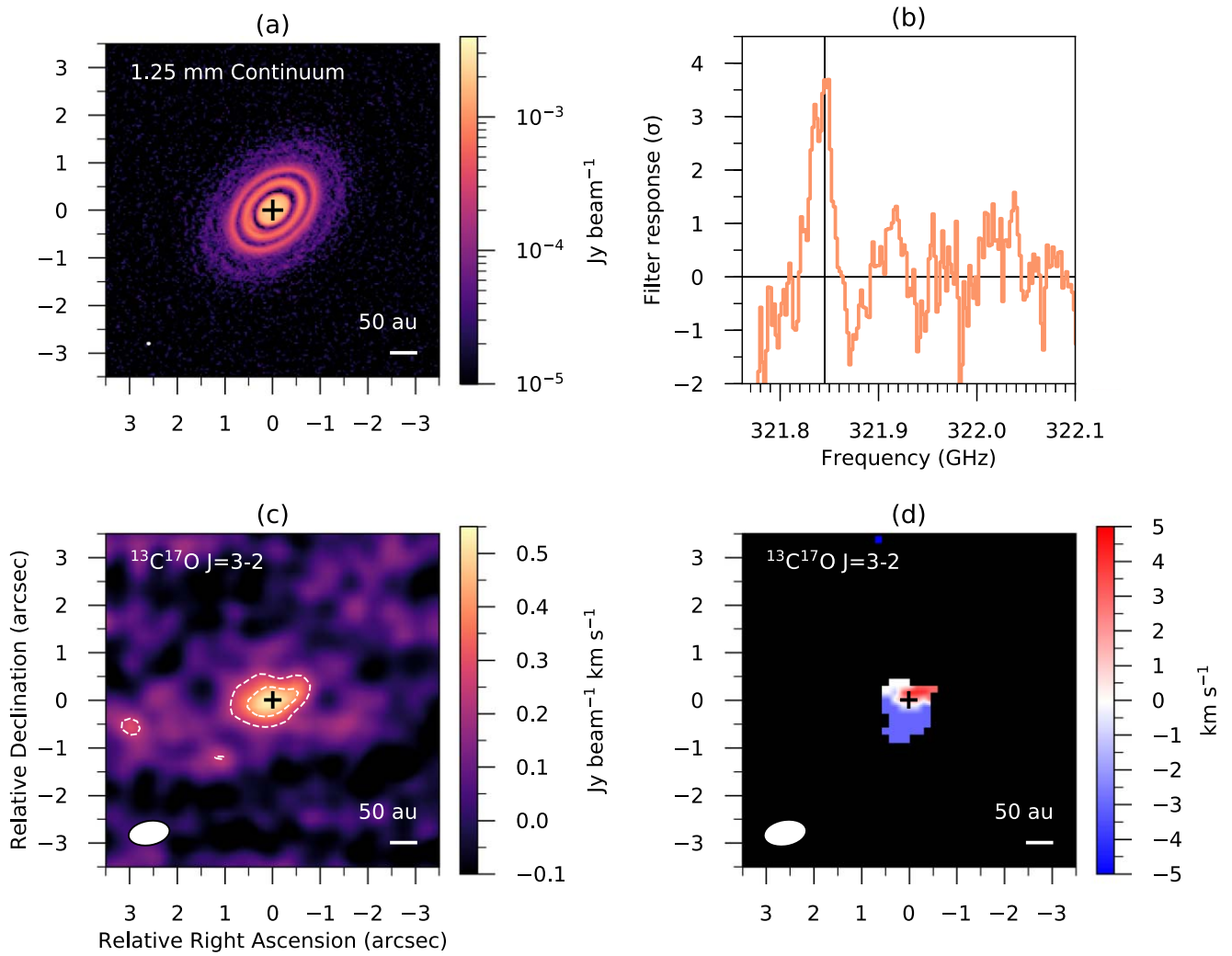
Figure 1. (a) The 1.25 mm continuum image from Isella et al. (2018). (b) The matched filter response for the $^{13}C^{17}O$ $J = 3$–2 detection where the black line marks the frequency of the hyperfine transitions. (c) The $^{13}C^{17}O$ $J = 3$–2 integrated intensity map where the white dashed contours mark 3σ and 5σ. (d) The $^{13}C^{17}O$ $J = 3$–2 intensity-weighted velocity map.

lines lie within a frequency range less than the spectral resolution of the data; hence, we are observing the blending of all of the lines. The $^{13}C^{17}O$ molecular data we use is from Klapper et al. (2003) and was accessed via the Cologne Database for Molecular Spectroscopy (CDMS; Müller et al. 2005). We detected $^{13}C^{17}O$ initially via a matched filter analysis[8] (Loomis et al. 2018) using a Keplerian mask assuming a disk position angle of 132° and an inclination of 42° (e.g., Isella et al. 2016). The resulting signal-to-noise ratio (S/N) is ≈3.5. The filter response is shown in Figure 1(b) with the black line marking the $^{13}C^{17}O$ $J = 3$–2 transition after correction for the source velocity (5.8 km s^{-1}).

The line imaging was conducted using CLEAN with CASA version 4.6.0. The native spectral resolution of the data is 1.8 km s^{-1}; however, in order to optimize the S/N the final images were generated with a 3 km s^{-1} channel width and a *uv* taper of 0″5 resulting in a synthesized beam of 0″87 × 0″51 (100°). Figures 1(c) and (d) present the $^{13}C^{17}O$ integrated intensity map and the intensity-weighted velocity map, respectively. The integrated intensity map was made

using channels ±6 km s^{-1} about the source velocity. The peak integrated intensity is 0.55 Jy beam^{-1} km s^{-1} with an rms noise level of 0.08 Jy beam^{-1} km s^{-1} (S/N = 7) that was extracted from the spatial region beyond the detected line emission. The intensity-weighted velocity map was made in the same manner but also with a 3σ clip.

We also use archival data to benchmark our modeling, including the $^{12}C^{16}O$, $^{13}C^{16}O$, $^{12}C^{18}O$ $J = 2$–1 transitions reported in Isella et al. (2016), and the $^{12}C^{16}O$ $J = 3$–2 ALMA Science Verification data.[9] All integrated intensity maps were deprojected and azimuthally averaged and are shown in Figures 3(a)–(e). The errors are the standard deviation of intensity of the pixels in each bin divided by the number of beams per annulus (e.g., Carney et al. 2018). In addition, Figure 3(e) shows the $^{12}C^{17}O$ $J = 3$–2 total integrated intensity value with its associated errors (Qi et al. 2011). All data plotted assume a source distance of 122 pc (van den Ancker et al. 1998). Although *GAIA* DR2 puts this source at 101.5 pc (Gaia Collaboration et al. 2018), in order to compare to previous analyses we use the previous value. We discuss the impact of the revised distance in Section 4.

---

[8] A python-based open-source implementation of VISIBLE is available at http://github.com/AstroChem/VISIBLE.

[9] https://almascience.nrao.edu/alma-data/science-verification

3. Analysis

Previous observations of the HD 163296 disk with the SMA and ALMA have detected multiple CO isotopologues: $^{12}\text{C}^{16}\text{O}$, $^{13}\text{C}^{16}\text{O}$, $^{12}\text{C}^{18}\text{O}$, and $^{12}\text{C}^{17}\text{O}$ (Qi et al. 2011; Isella et al. 2016). The models that were used to reproduce the line emission in Qi et al. (2011) recover the following global isotope ratios:

$$n(^{12}\text{C}^{16}\text{O})/n(^{13}\text{C}^{16}\text{O}) = 67 \pm 8,$$

$$n(^{12}\text{C}^{16}\text{O})/n(^{12}\text{C}^{18}\text{O}) = 444 \pm 88,$$

$$n(^{12}\text{C}^{18}\text{O})/n(^{12}\text{C}^{17}\text{O}) = 3.8 \pm 1.7,$$

where $n(^{X}\text{C}^{Y}\text{O})$ is the number density of the molecule. This is consistent with the carbon and oxygen isotope ratios observed in the ISM (Wilson 1999).

We make a first estimate of the column density of gas traced by the $^{13}\text{C}^{17}\text{O}$ emission under the assumption of optically thin emission in local thermodynamic equilibrium. Following Carney et al. (2019, their Equation (1), with molecular data obtained from CDMS; Müller et al. 2005), the average column density for the $^{13}\text{C}^{17}\text{O}$ within 50 au, assuming an excitation temperature of 50 K, is 7.1×10^{15} cm^{-2}. This is equivalent to an n_{H} column density of 2.65×10^{25} cm^{-2} (44.4 g cm^{-2}) at 50 au. In comparison, the corresponding value for the $^{12}\text{C}^{18}\text{O}$ is 1.7×10^{16} cm^{-2}, resulting in an $n(^{12}\text{C}^{18}\text{O})/n(^{13}\text{C}^{17}\text{O})$ ratio of 2.5. Under the assumption that both the lines are optically thin (and taking the previously derived isotopic ratios), this value is a factor of 100 too small. Therefore, the $^{12}\text{C}^{18}\text{O}$ line emission is optically thick and the resulting gas mass derived from this tracer will be underestimated.

To quantify this more robustly, we utilize an existing disk model that has been shown to fit emission lines from multiple CO isotopologues ($^{12}\text{C}^{16}\text{O}$, $^{13}\text{C}^{16}\text{O}$, $^{12}\text{C}^{18}\text{O}$, and $^{12}\text{C}^{17}\text{O}$) to model our $^{13}\text{C}^{17}\text{O}$ detection (Qi et al. 2011). The density (hydrogen nuclei density, n_{H}) and temperature of the disk are shown in Figures 2(a) and (b). The CO abundance distribution, shown in Figure 2(c), was determined by setting $n(\text{CO})$ to a constant fractional abundance of 6.0×10^{-5} with respect to H$_2$ in the molecular layer following Qi et al. (2011). This assumes that 41% of volatile carbon is in the form of CO (Graedel et al. 1982). This abundance was reduced by a factor of 10^{-4} in the midplane where $T_{\text{gas}} \leqslant 19$ K and by a factor of 10^{-8} in the atmosphere where the vertically integrated hydrogen column density, $\sigma(n_{\text{H}})$, from the disk surface is $<1.256 \times 10^{21}$ cm^{-2}. The depleted value in the midplane is consistent with the CO abundances derived from chemical models including nonthermal desorption (Walsh et al. 2010). The photodissociation and freezeout boundaries are shown in white contours overlaid on Figures 2(a) and (b).

The first model that we test, Model 1, uses a constant $^{13}\text{C}^{17}\text{O}$ fractional abundance of 5.39×10^{-10} relative to H$_2$. This assumes isotope ratios that are consistent with the observations and modeling from Qi et al. (2011). Model 1 has a total disk mass of 0.089 $M_{\odot}$. Using the CDMS data for $^{13}\text{C}^{17}\text{O}$ we generated a LAMDA-like file in order to model the $J = 3$–2 hyperfine components in the Line Modeling Engine (LIME[10]; Brinch & Hogerheijde 2010). Synthetic images cubes were computed assuming the appropriate position angle and inclination of the source, and the resulting images were smoothed with a Gaussian beam to the spatial resolution of the observations using the CASA task, IMSMOOTH. The generated

integrated intensity map was then deprojected and azimuthally averaged. The radial profiles from Model 1 (orange) are shown alongside the observations in Figures 3(a)–(e).

Model 1 underpredicts the $^{13}\text{C}^{17}\text{O}$ peak emission in the integrated intensity map by a factor of 2.5, yet provides a reasonable fit to the other lines (within a factor of two). The higher spatial resolution observations are effected by dust opacity within $\approx$50 au (see Isella et al. 2016); therefore, we focus on reproducing the data beyond 50 au.

To better fit the $^{13}\text{C}^{17}\text{O}$ observations we globally increase the gas mass of Model 1. This was done by initially multiplying n_{H} by a factor of 1.5 and then increasing this factor in steps of 0.5 until the best by-eye fit of 3.5 was found. The results for Model 2 are shown in Figure 3 (purple). Model 2 provides a better fit to all of the lines. This model assumes a smooth radial gas density structure contrary to the most recent observations. However, our work is focused on reproducing the global disk mass rather than the underlying small-scale gas surface density variations. Model 2 has a total disk mass of 0.31 $M_{\odot}$.

We note that a similar fit can be obtained using a different CO snow-line location at 90 au as determined in Qi et al. (2015). This requires a corresponding increase in gas mass ($\times$3.5) within the snow line, and we obtain a similar $^{12}\text{C}^{18}\text{O}$ column density profile as in Qi et al. (2015) beyond the snow line. Both of these models use the same underlying physical structure but have different CO snow-line locations and levels of CO depletion beyond the snow line. The Qi et al. (2011) model has simpler assumptions regarding the freezeout of CO, consistent with other work (e.g., Williams & Best 2014), and was found to be a slightly better fit to the observations.

We also generated optical depth maps for a face-on disk to recover the maximum value of τ for each transition. We then radially averaged these maps and plotted the resulting optical depth of the $^{12}\text{C}^{18}\text{O}$ $J = 2$–1 and $^{13}\text{C}^{17}\text{O}$ $J = 3$–2 transitions for both models in Figure 2(d). It can be seen that $^{12}\text{C}^{18}\text{O}$ is optically thick within the CO snow line (155 au) in both models, whereas the $^{13}\text{C}^{17}\text{O}$ remains optically thin across the full radial extent of the disk.

4. Discussion

4.1. Comparison to Other Mass Estimates

Using observations of $^{13}\text{C}^{17}\text{O}$ we derive a new gas mass for the HD 163296 disk of 0.31 $M_{\odot}$. The total disk mass depends on the gas-to-dust mass ratio (g/d), and using the dust mass from Isella et al. (2007) we find a g/d $\approx$ 260. Here we compare our results to previous works.

The HD 163296 disk has been well studied and there are many mass measurements in the literature. In general, our estimate is the highest by a factor of 2–6 compared to previous studies using $^{12}\text{C}^{18}\text{O}$ (e.g., 0.17 $M_{\odot}$ and 0.048 $M_{\odot}$ from Isella et al. 2007 and Williams & McPartland 2016, respectively). There are a range of g/d values in the literature that span four orders of magnitude. Tilling et al. (2012) and Boneberg et al. (2016) models require a low g/d = 20. Isella et al. (2016) have a radially varying g/d covering a range from $\approx$30 to $\approx$1100. Recent work from Powell et al. (2019) recovers a total disk mass of 0.21 $M_{\odot}$ with a high g/d $\sim 10^4$ in the outer disk. The one documented mass higher than our result is 0.58 $M_{\odot}$ with a g/d = 350 (Woitke et al. 2019). The inconsistencies in these mass measurements and g/d from different models may be explained by trying to recover the gas density structure with
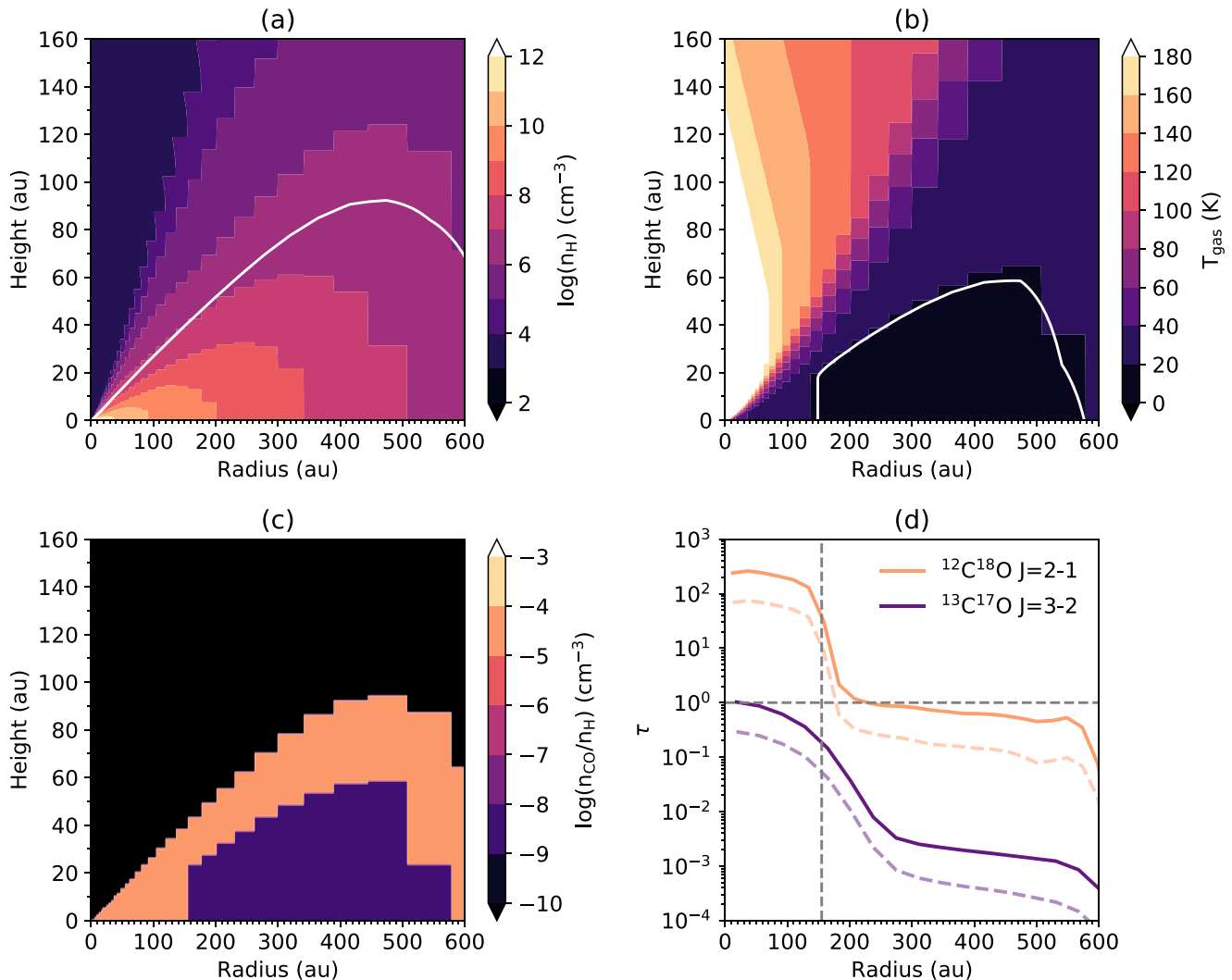
---

[10] https://github.com/lime-rt/lime

Figure 2. Disk physical structure from Qi et al. (2011). (a) The n_H density. (b) The gas temperature. The white contours mark $\Sigma(n_H) = 1.256 \times 10^{21}$ cm^{-2} and $T_{gas} = 19$ K, respectively. (c) The $n(CO)/n_H$ distribution. (d) The radially averaged optical depth (τ) of the $^{12}C^{18}O$ $J = 2$–1 and $^{13}C^{17}O$ $J = 3$–2 transitions from Model 1 (light purple and orange dashed lines) and Model 2 (dark purple and orange solid lines) assuming a face-on disk. The vertical dashed line marks the location of the CO snow line in both models (155 au) and the horizontal dashed line marks where $\tau = 1$.

optically thick lines. CO remains the best and most accessible tracer of mass that we have for disks (Molyarova et al. 2017), but robust lower limits to the gas mass can only be made by targeting the most optically thin isotopologues ($^{12}C^{17}O$, $^{13}C^{18}O$, and $^{13}C^{17}O$).

These masses have all been determined using a source distance of 122 pc. Considering the revised distance of 101.5 pc, the total disk gas mass from our work is thus 0.21 $M_\odot$ (mass ∝ flux ∝ distance^2).

4.2. The Impact of CO Chemistry on the Disk Mass

CO is susceptible to isotope-selective photodissociation that can reduce the abundance of the rarer isotopologues relative to $^{12}C^{16}O$ in the disk atmosphere. We find that the observations are well fit with interstellar isotopic abundances. Because the $^{12}C^{16}O$, $^{13}C^{16}O$, and $^{12}C^{18}O$ line emission is optically thick, testing the significance of isotope-selective photodissociation in this disk requires higher-sensitivity observations of the rarer isotopologues.

Observations have shown that CO is depleted with respect to H$_2$ in disks; however, without a better tracer of the H$_2$ column

density, e.g., HD, the level of depletion is difficult to constrain. Carbon depletion effects are less significant in warmer disks around Herbig Ae stars compared to their T Tauri counterparts. Observations show moderate carbon depletion in the Herbig disk around HD 100546 with a model-derived [C]/[H] abundance ratio of $(0.1$–$1.5) \times 10^{-4}$ (Kama et al. 2016), and the value for CO adopted in our model is within this range. Consistent with this, models have also suggested that these disks have a close to canonical $n(CO)/n(H2)$ abundance (Bosman et al. 2018). These two chemical effects (isotope-selective photodissociation and carbon depletion) imply that our gas mass estimate is a lower limit. We note that after Zang et al. (2019) recently showed that the HD163296 disk has modest carbon depletion that is similar to the HD100546 disk, and that the CO abundance is slightly enhanced within the CO snowline. Further observations of the optically thin CO isotopologues would confirm this.

4.3. Constraints on the Location of the CO Snow Line

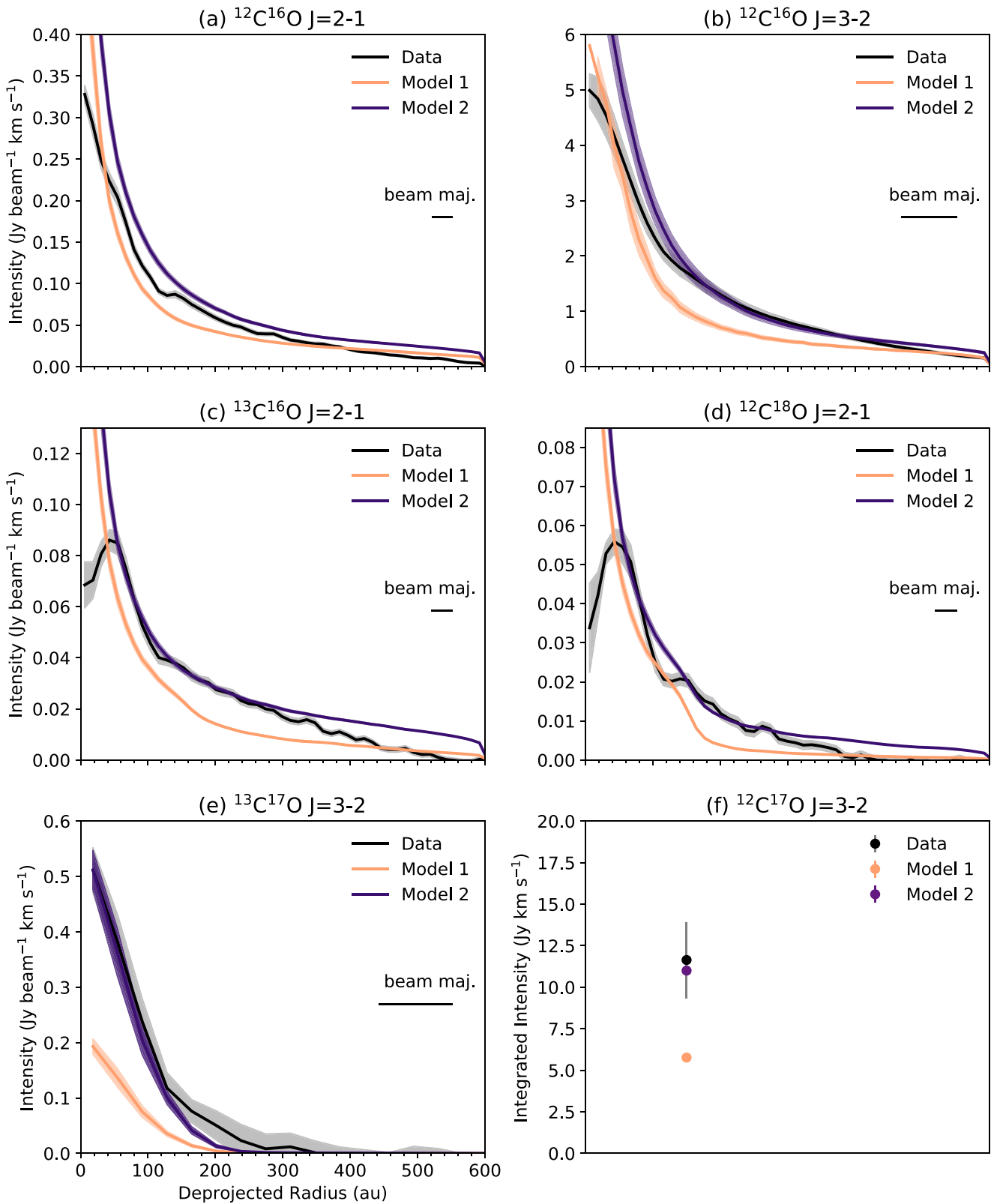Locating the midplane CO snow line in disks is difficult due to the high optical depth of the more abundant CO

Figure 3. ((a)–(e)) The deprojected and azimuthally averaged radial profiles of the observed and modeled CO lines. (f) The value of integrated flux of the observed and modeled C^{17}O $J = 3$–2 line. The shaded regions are the errors as described in the text. Model 1 has a total disk mass of 0.089 $M_\odot$, and Model 2 has a total disk mass of 0.31 $M_\odot$.

isotopologues and the vertical temperature gradient of the disk. The location of the CO snow line can be determined directly by observing less abundant, optically thin, CO isotopologues, or by detecting molecules that, due to chemistry, peak in abundance at a location related to the snow line. Qi et al. (2011) use observations CO and put the snow line at 155 au at 19 K: follow-up work suggested that the snow line was instead at 90 au and 25 K (Qi et al. 2015). Out of these two scenarios

our $^{13}C^{17}O$ observations fit best with the former option given the data in hand. The relationship between the cations, DCO^+ (ring from 110 and 160 au) and N_2H^+ (inner edge of the ring at 90 au), and the location of the midplane CO snow line are not trivial, but both species have been detected in this disk (Mathews et al. 2013; Qi et al. 2015). Our analysis shows that the $C^{18}O$ emission in both models tested is optically thick, and thus cannot be used to easily locate the midplane CO snow line. However, the $^{13}C^{17}O$ emission is optically thin, so future observations at a higher spatial resolution and sensitivity could be used to directly constrain the radius of the midplane CO snow line. The new source distance from *GAIA* puts the proposed snow-line locations at 75 and 128 au. The former location is close to one of the observed dust gaps in the disk, and it may be the case that the drop in CO surface density detected here is due to gas depletion rather than the snow line. It is important to note that the snow line is not a simple sharp transition at the condensation temperature, but is instead determined by the balance of the rates of freezeout and thermal desorption, which should be considered in future disk models.

4.4. Is the Disk Gravitationally Stable?

The potential exoplanet population currently probed with ALMA, via the ringed depletion of continuum emission, is gas giant planets on wide orbits. In the case of HD 163296 this would imply a multiple giant planet system and indeed, the presence of such a system has already been proposed (Isella et al. 2016; Liu et al. 2018; Pinte et al. 2018; Teague et al. 2018). The formation of massive planets on wide orbits can in some cases be achieved by core accretion, but a more economical route might involve the gravitational fragmentation of the outer regions of the disk (Boss 2011). Our new, higher disk mass estimate prompts us to investigate whether such processes may have occurred (or be occurring) in the HD 163296 disk.

The stability of a disk against fragmentation can be quantified via the Toomre Q parameter (Toomre 1964):

$$Q = \frac{c_s \kappa}{\pi G \Sigma},$$

where c_s is the sound speed of the gas, κ is the epicyclic frequency (equal to the angular velocity Ω in a Keplerian disk), and Σ is the surface density of the gas. Toomre Q values of 1 or less imply that the disk is susceptible to fragmentation, but simulations have shown that disks with $Q \lesssim 1.7$ begin to undergo instabilities in the form of nonaxisymmetric spirals (Durisen et al. 2007). We calculate Q across the disk (Figure 4, orange) accounting for the lower mass due to the new source distance, assuming a g/d of 260, and the midplane temperature structure of our model (Figure 2(b)). We find that the minimum value of Q is ≈ 6 at ≈ 110 au, suggesting that the disk is currently gravitationally stable (in agreement with recent work from Powell et al. 2019).

The relatively large age of the HD 163296 system brings into question its stability earlier in its lifetime. The determination of previous disk masses is complicated by processes including episodic accretion (e.g., Mendigutía et al. 2013) and the decrease in accretion rate with time (e.g., Venuti et al. 2014). The magnitude of these effects are still under debate (see Hartmann et al. 2016 for a review), so we therefore assume that all of the accreted mass once resided in the disk, and that the
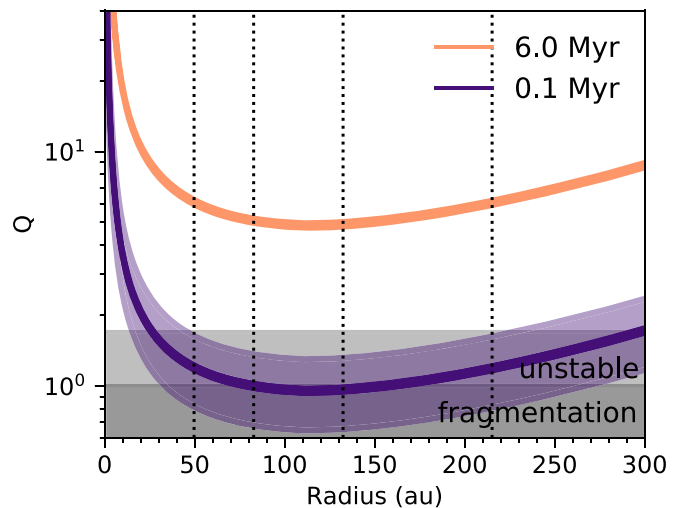

Figure 4. Toomre Q parameter for the new disk mass we derive in Model 2 and extrapolated back to 0.1 Myr. The shaded regions incorporate both the errors in stellar age and mass accretion rate. Vertical dashed lines mark the radial positions of gaps in the millimeter dust and kinematic perturbations that may be due to protoplanets.

accretion rate ($\dot{M}$) has been constant over the disk lifetime. HD 163296 has an estimated age of $6.03^{+0.43}_{-0.14}$ Myr and $\log \dot{M} = -6.81^{+0.16}_{-0.15} M_\odot \, yr^{-1}$ (C. Wichittanakom et al. 2019, in preparation); thus, under these assumptions, we estimate the disk mass at 0.1 Myr to be $1.13^{+0.51}_{-0.28} M_\odot$.

The resulting minimum Toomre Q values for this star–disk configuration[11] would be in the range of 1.3–0.7 (Figure 4, purple), placing regions of the disk from ∼50–220 au in the regime of instability. Such behavior early in the disk lifetime has implications for the trapping and growth of dust (Rice et al. 2004) and the chemical composition of the disk (Evans et al. 2015). This previous unstable state could also be the source of the four massive planets currently proposed to reside in the disk around HD 163296.

5. Conclusions

We have presented the first detection of $^{13}C^{17}O$ in a protoplanetary disk showcasing the power of this optically thin isotopologue as a tracer of disk gas mass. This work provides robust evidence that disks are more massive than previously assumed (see also Zhu et al. 2019). Future observations of this tracer in more sources may help to address the discrepancy between the masses of disks and the observed exoplanet population (Manara et al. 2018).

---

[11] We note this does not account for any change in the stellar mass over this time period, which would decrease Q further.

ORCID iDs

Alice S. Booth ⓘ https://orcid.org/0000-0003-2014-2121
Catherine Walsh ⓘ https://orcid.org/0000-0001-6078-786X
John D. Ilee ⓘ https://orcid.org/0000-0003-1008-1142
Shota Notsu ⓘ https://orcid.org/0000-0003-2493-912X
Chunhua Qi ⓘ https://orcid.org/0000-0001-8642-1786
Hideko Nomura ⓘ https://orcid.org/0000-0002-7058-7682
Eiji Akiyama ⓘ https://orcid.org/0000-0002-5082-8880

References

Ansdell, M., Williams, J. P., van der Marel, N., et al. 2016, ApJ, 828, 46
Bergin, E. A., Cleeves, L. I., Gorti, U., et al. 2013, Natur, 493, 644
Bergin, E. A., & Williams, J. P. 2017, in Formation, Evolution, and Dynamics of Young Solar Systems, Astrophysics and Space Science Library, Vol. 445,, ed. M. Pessah & O. Gressel (Berlin: Springer), 1
Boneberg, D. M., Panić, O., Haworth, T. J., Clarke, C. J., & Min, M. 2016, MNRAS, 461, 385
Bosman, A. D., Walsh, C., & van Dishoeck, E. F. 2018, A&A, 618, A182
Boss, A. P. 2011, ApJ, 731, 74
Brinch, C., & Hogerheijde, M. R. 2010, A&A, 523, A25
Carney, M. T., Fedele, D., Hogerheijde, M. R., et al. 2018, A&A, 614, A106

Carney, M. T., Hogerheijde, M. R., Guzmán, V. V., et al. 2019, A&A, 623, A124
Durisen, R. H., Boss, A. P., Mayer, L., et al. 2007, in Protostars and Planets V, ed. B. Reipurth, D. Jewitt, & K. Keil (Tucson, AZ: Univ. Arizona Press), 607
Evans, M. G., Ilee, J. D., Boley, A. C., et al. 2015, MNRAS, 453, 1147
Gaia Collaboration, Brown, A. G. A., Vallenari, A., et al. 2018, A&A, 616, A1
Graedel, T. E., Langer, W. D., & Frerking, M. A. 1982, ApJS, 48, 321
Hartmann, L., Herczeg, G., & Calvet, N. 2016, ARA&A, 54, 135
Isella, A., Guidi, G., Testi, L., et al. 2016, PhRvL, 117, 251101
Isella, A., Huang, J., Andrews, S. M., et al. 2018, ApJL, 869, L49
Isella, A., Testi, L., Natta, A., et al. 2007, A&A, 469, 213
Kama, M., Bruderer, S., van Dishoeck, E. F., et al. 2016, A&A, 592, A83
Klapper, G., Surin, L., Lewen, F., et al. 2003, ApJ, 582, 262
Liu, S.-F., Jin, S., Li, S., Isella, A., & Li, H. 2018, ApJ, 857, 87
Long, F., Herczeg, G. J., Pascucci, I., et al. 2017, ApJ, 844, 99
Loomis, R. A., Öberg, K. I., Andrews, S. M., et al. 2018, AJ, 155, 182
Manara, C. F., Morbidelli, A., & Guillot, T. 2018, A&A, 618, L3
Mathews, G. S., Klaassen, P. D., Juhász, A., et al. 2013, A&A, 557, A132
McClure, M. K., Bergin, E. A., Cleeves, L. I., et al. 2016, ApJ, 831, 167
Mendigutía, I., Brittain, S., Eiroa, C., et al. 2013, ApJ, 776, 44
Miotello, A., Bruderer, S., & van Dishoeck, E. F. 2014, A&A, 572, A96
Molyarova, T., Akimkin, V., Semenov, D., et al. 2017, ApJ, 849, 130
Müller, H. S. P., Schlöder, F., Stutzki, J., & Winnewisser, G. 2005, JMoSt, 742, 215
Notsu, S., Akiyama, E., Booth, A., et al. 2019, ApJ, 875, 96
Pinte, C., Price, D. J., Ménard, F., et al. 2018, ApJL, 860, L13
Powell, D., Murray-Clay, R., Pérez, L. M., Schlichting, H. E., & Rosenthal, M. 2019, ApJ, 878, 116
Qi, C., D'Alessio, P., Öberg, K. I., et al. 2011, ApJ, 740, 84
Qi, C., Öberg, K. I., Andrews, S. M., et al. 2015, ApJ, 813, 128
Rice, W. K. M., Lodato, G., Pringle, J. E., Armitage, P. J., & Bonnell, I. A. 2004, MNRAS, 355, 543
Teague, R., Bae, J., Bergin, E. A., Birnstiel, T., & Foreman-Mackey, D. 2018, ApJL, 860, L12
Tilling, I., Woitke, P., Meeus, G., et al. 2012, A&A, 538, A20
Toomre, A. 1964, ApJ, 139, 1217
van den Ancker, M. E., de Winter, D., & Tjin A Djie, H. R. E. 1998, A&A, 330, 145
Venuti, L., Bouvier, J., Flaccomio, E., et al. 2014, A&A, 570, A82
Walsh, C., Millar, T. J., & Nomura, H. 2010, ApJ, 722, 1607
Williams, J. P., & Best, W. M. J. 2014, ApJ, 788, 59
Williams, J. P., & McPartland, C. 2016, ApJ, 830, 32
Wilson, T. L. 1999, RPPh, 62, 143
Woitke, P., Kamp, I., Antonellini, S., et al. 2019, PASP, 131, 064301
Zhang, K., Bergin, E. A., Blake, G. A., Cleeves, L. I., & Schwarz, K. R. 2017, NatAs, 1, 0130
Zhang, K., Bergin, E. A., Schwarz, K. R., Krijt, S., & Ciesla, F. 2019, ApJ, (arXiv:1908.03267)
Zhu, Z., Zhang, S., Jiang, Y.-F., et al. 2019, ApJL, 877, L18